INTERNATIONAL JOURNAL FOR NUMERICAL METHODS IN FLUIDS, VOL. 10, 771–790 (1990)

FINITE VOLUME METHOD FOR PREDICTION OF FLUID FLOW IN ARBITRARILY SHAPED DOMAINS WITH MOVING BOUNDARIES

I. DEMIRDŽIĆ

Mašinski Fakultet Univerziteta u Sarajevu, Omladinsko šetalište bb, YU-71000 Sarajevo, Yugoslavia

AND

M. PERIĆ

Lehrstuhl für Strömungsmechanik, Universität Erlangen-Nürnberg, Egerlandstr. 13, D-8520 Erlangen, Federal Republic of Germany

SUMMARY

In this paper a method is presented that can be used for both the Lagrangian and the Eulerian solution of the Navier–Stokes equations in a domain of arbitrary shape, bounded by boundaries which move in any prescribed time-varying fashion. The method uses the integral form of the governing equations for an arbitrary moving control volume, with pressure and Cartesian velocity components as dependent variables. Care is taken to also satisfy the space conservation law, which ensures a fully conservative computational procedure. Fully implicit temporal differencing makes the method stable for any time step.

A detailed description is provided for the discretization in two dimensions, with a collocated arrangement of variables. Central differences are used to evaluate both the convection and diffusion fluxes. The well known SIMPLE algorithm is employed for pressure–velocity coupling. The resulting algebraic equation systems are solved iteratively in a sequential manner. Results are presented for a flow in a channel with a moving indentation; they show favourable agreement with experimental observations.

KEY WORDS Finite volume Conservative Prediction Fluid flow Moving grid

INTRODUCTION

There are many kinds of fluid flow which are best studied in a non-Eulerian co-ordinate system, as is the case with flows in domains with moving boundaries. There are also cases where the use of such a co-ordinate system may be desirable for computational convenience, e.g. in calculations on adaptive numerical grids.

Flows with moving boundaries can be encountered in many practical situations; among those in which considerable research interest has been shown in recent years are in-cylinder flows in internal combustion engines, free surface flows, flows in blood vessels, etc. The main feature of these flows is their unsteadiness, both with respect to flow patterns and to the shape of the boundary and the conditions which apply there. Whilst many numerical solutions of unsteady flows have been presented in the literature, problems with moving boundaries have been considered by relatively few authors. Viecelly[1] used a modified version of the MAC procedure of

0271–2091/90/070771–20$10.00

Received November 1988
Revised August 1989

Harlow and Welch[2] to solve the same free surface and 'flexible bag' problems; Godunov and Prokopov[3] developed a two-dimensional finite difference moving mesh method for compressible flow calculations; Hirt *et al.*[4] presented a general method for the solution of both compressible and incompressible flow problems; Gosman and Watkins,[5] Gosman and Johns[6] and Gosman[7] reported calculations of in-cylinder flows; Thomas and Lombard[8] presented solutions of steady and unsteady supersonic flow equations; Ling and Atabek[9] used an approximate numerical method for the calculation of flow in arteries; Krause[10] presented some calculations of incompressible viscous flow in vessels with moving boundaries; Ralph and Pedley[11] modified the streamfunction–vorticity equations and a finite difference solution scheme to obtain a solution for laminar flow in a channel with moving indentation; etc. Most of the solution methods presented in the cited references are applicable only to a certain class of problems for which they have been specially designed (rectangular grid, only one set of grid lines moves, etc.). When only one of the solution domain boundaries moves in one direction, simple transformation of the conservation equations allows for easy discretization (e.g. in Gosman[7] and Durst *et al.*[12]). However, in a general case when grid movement in all directions can take place simultaneously, careful discretization is necessary in order to satisfy the space conservation law. Demirdžić and Perić[13] have shown that failure to do so introduces errors in the form of artificial mass sources.

Adaptation of grid lines to the flow direction enables achievement of higher accuracy at the same level of grid fineness. It is especially desirable in supersonic flow problems, where high gradients in the shock region need very fine grids to be adequately resolved. Some such applications are presented in Thompson;[14] also by Deiwert and Rothmund,[15] Hung and Buning[16] and others. However, most of the grid adaptation methods were used in conjunction with steady flow calculations, in which case it is not necessary to have a moving grid. In an iterative solution procedure the grid adaptation can be performed between two iterations, and the solution procedure can continue without taking into account the old grid position. When the flow is unsteady, the grid adaptation has to be performed between two time steps, and the movement of grid lines has to be properly accounted for in the discretization scheme.

When the grid moves to adapt to the new flow field, one has to devise a strategy or criteria according to which this movement should take place. This is a very complex issue, and further discussion of it is beyond the scope of this study (some approaches are discussed in Thompson[14]). We focus our attention on the implementation of the moving grid concept into a finite volume discretization scheme for general boundary-fitted grids. The laws which govern the grid movement are, for the sake of this task, irrelevant; here we take it simply that the grid is required to fit the boundary and that the position of the boundary is known at each time step.

The solution method to be presented in this paper is an extension of the method developed for steady flows by Perić.[17] The novelty is the implementation of the moving grid concept in a way which ensures the satisfaction of the space conservation law (SCL), whose importance in numerical calculations with moving grids has been demonstrated in an earlier publication.[13] A convenient collocated variable arrangement is employed, with second-order central differencing in space and first-order fully implicit differencing in time. For the sake of brevity the method is described for two-dimensional problems; its extension to three dimensions is, however, straightforward.

The next section describes briefly the governing equations for the unsteady flow in a moving co-ordinate frame. The following section describes the discretization procedure adopted by the authors. Application of the solution method developed here to a two-dimensional problem of laminar flow in a channel with moving indentation is then presented. Finally, conclusions are drawn and possibilities of further development of the solution scheme are presented.

GOVERNING EQUATIONS

In order to describe the fluid flow and related transport phenomena in moving (non-Eulerian) co-ordinates, we use the integral form of the conservation laws for space, mass, momentum and scalar quantities (thermal energy, concentration, etc.), which for an arbitrary spatial region (of the Euclidean space) of volume V bounded by a closed surface S can be written[18]

$$\frac{\mathrm{d}}{\mathrm{d}t}\int_V \mathrm{d}V - \int_S \mathbf{v}_\mathrm{b}\cdot\mathrm{d}\mathbf{S} = 0, \tag{1a}$$

$$\frac{\mathrm{d}}{\mathrm{d}t}\int_V \rho\,\mathrm{d}V + \int_S \rho(\mathbf{v}-\mathbf{v}_\mathrm{b})\cdot\mathrm{d}\mathbf{S} = 0, \tag{1b}$$

$$\frac{\mathrm{d}}{\mathrm{d}t}\int_V \rho v\,\mathrm{d}V + \int_S [\rho(\mathbf{v}-\mathbf{v}_\mathrm{b})\mathbf{v} - \boldsymbol{T}]\cdot\mathrm{d}\mathbf{S} = \int_V \mathbf{s}_v\,\mathrm{d}V, \tag{1c}$$

$$\frac{\mathrm{d}}{\mathrm{d}t}\int_V \rho\phi\,\mathrm{d}V + \int_S [\rho(\mathbf{v}-\mathbf{v}_\mathrm{b})\phi - \mathbf{q}]\cdot\mathrm{d}\mathbf{S} = \int_V s_\phi\,\mathrm{d}V, \tag{1d}$$

where ρ represents the fluid density, $\mathbf{v}$ is the fluid velocity, $\mathbf{v}_\mathrm{b}$ is the velocity of the boundary of a control volume, ϕ stands for any scalar quantity (enthalpy, concentration, etc.), $\mathbf{s}_v$ and s_ϕ are the volumetric sources of momentum and scalar quantity respectively, and the stress tensor and flux vector are, for a Newtonian fluid, defined respectively as

$$\boldsymbol{T} = -(p + \tfrac{2}{3}\mu\,\mathrm{div}\,\mathbf{v})\boldsymbol{I} + 2\mu\boldsymbol{D}, \tag{2}$$

$$\mathbf{q} = \Gamma_\phi\,\mathrm{grad}\,\phi. \tag{3}$$

Here p is the pressure, μ is the dynamic viscosity of the fluid, Γ_ϕ is the diffusion coefficient for the transported quantity ϕ, $\boldsymbol{I}$ is the unit tensor and $\boldsymbol{D}$ stands for the rate-of-strain (deformation) tensor, defined as

$$\boldsymbol{D} = \tfrac{1}{2}[\mathrm{grad}\,\mathbf{v} + (\mathrm{grad}\,\mathbf{v})^\mathrm{T}]. \tag{4}$$

From the momentum conservation equation (1c), equations for the Cartesian velocity components u_i are obtained by taking a dot product of it and the corresponding base vector $\mathbf{i}_i$; thus

$$\frac{\mathrm{d}}{\mathrm{d}t}\int_V \rho u_i\,\mathrm{d}V + \int_S [\rho(\mathbf{v}-\mathbf{v}_\mathrm{b})u_i - \mathbf{t}_i]\cdot\mathrm{d}\mathbf{S} = \int_V s_u\,\mathrm{d}V, \tag{5}$$

where (see equations (2) and (4))

$$\mathbf{t}_i = \boldsymbol{T}\cdot\mathbf{i}_i = -(p + \tfrac{2}{3}\mu\,\mathrm{div}\,\mathbf{v})\mathbf{i}_i + \mu\,\mathrm{grad}\,u_i + \mu(\mathrm{grad}\,\mathbf{v})^\mathrm{T}\cdot\mathbf{i}_i. \tag{6}$$

A particular feature of the conservation equations related to a control volume with a moving boundary is the fact that the convective fluxes through the control surface are expressed via the relative velocity $\mathbf{v} - \mathbf{v}_\mathrm{b}$, where the surface velocity $\mathbf{v}_\mathrm{b}$ has to satisfy the space conservation law.[13]

DISCRETIZATION PROCEDURE

The conservation equations (1a)–(1d) are discretized by employing a finite volume approach and a fully implicit temporal differentiation. The time step δt is first chosen, and the flow domain is subdivided into a finite number of contiguous control volumes (CV) of volume V bounded by cell faces S_j; see Figure 1. The computational points (nodes) are placed in the centre of each CV, as

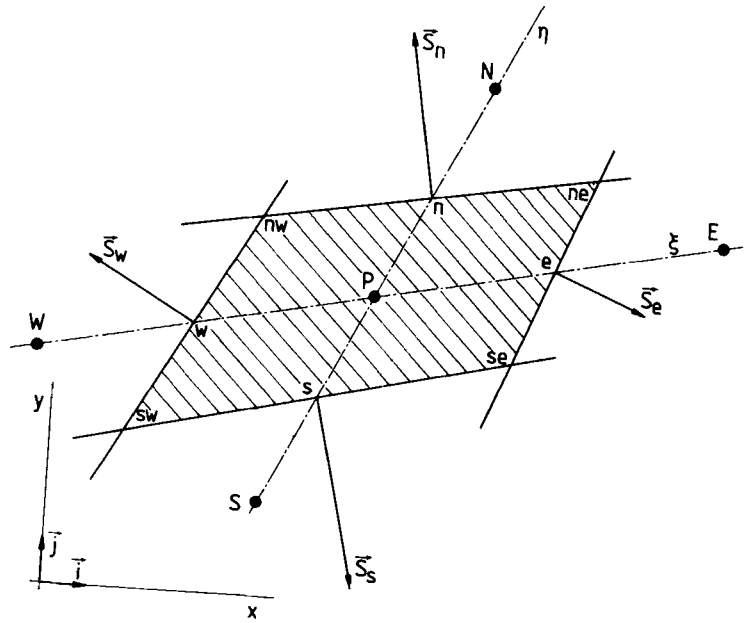

Figure 1. Two-dimensional control volume and labelling scheme

shown in Figure 1; boundary nodes, needed for the specification of boundary conditions, reside in the centre of boundary CV faces. All the dependent variables share the same storage location (collocated arrangement).

It is noted first that the SCL, equation (1a), can be solved explicitly at each CV face for the boundary velocity $\mathbf{v}_b$, as explained in detail by Demirdžić and Perić.[13] Alternatively, one can use this equation to calculate the volume fluxes through the CV faces which result from its motion. By assuming that the positions of a control volume at the two successive time steps are known, the SCL equation

$$\frac{\mathrm{d}}{\mathrm{d}t}\int_V \mathrm{d}V - \sum_j \int_{S_j} \mathbf{v}_b \cdot \mathrm{d}\mathbf{S} = 0, \quad j = \mathrm{e, w, n, s}, \tag{7}$$

can be discretized in the following way:

$$\frac{V^n - V^o}{\delta t} = \frac{\delta V}{\delta t} = \frac{\Sigma \delta V_j}{\delta t} = \sum_j (\mathbf{v}_b \cdot \mathbf{S})_j. \tag{8}$$

In the above expression V^n and V^o are the cell volumes at the new and old time levels respectively, and δV_j represents the volume swept by the jth CV face during time δt, as indicated by the shaded area in Figure 2. The latter can easily be calculated when the co-ordinates of the CV vertices are known at both time levels, as assumed here.

All the other conservation equations have the same general form, represented by the scalar equation (1d). By taking into account the shape of the control volumes, the representative conservation equation to be discretized can, for a given CV, be written as

$$\underset{\text{rate of change}}{\frac{\mathrm{d}}{\mathrm{d}t}\int_V \rho\phi \mathrm{d}V} + \underset{\text{convection}}{\sum_j \int_{S_j} [\rho(\mathbf{v}-\mathbf{v}_b)\phi]} - \underset{\text{diffusion}}{\Gamma_\phi \operatorname{grad}\phi] \cdot \mathrm{d}\mathbf{S}} = \underset{\text{source}}{\int_V s_\phi \mathrm{d}V}, \tag{9}$$

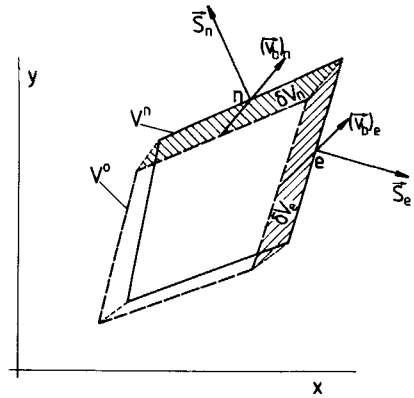

Figure 2. On the discretization of the SCL equation (7)

with four distinctive parts: rate of change, convection, diffusion and source (the mass conservation equation does not have a diffusion term). The rate-of-change and source terms are integrated over the cell volume, whereas the convection and diffusion terms form the sum of fluxes through the CV faces. The evaluation of each term will now be described.

Rate of change

It is taken that the value of the dependent variable ϕ in the middle of the control volume (computational node, point P in Figure 1) represents an average over the CV as a whole. Thus the rate-of-change term can be discretized as follows:

$$\frac{\mathrm{d}}{\mathrm{d}t}\int_V \rho\phi \mathrm{d}V \approx \frac{(\rho\phi V)_\mathrm{p}^\mathrm{n} - (\rho\phi V)_\mathrm{p}^\mathrm{o}}{\delta t}. \tag{10}$$

Here superscripts 'n' and 'o' denote the new and old time levels respectively. Since a fully implicit time discretization will be used, the superscript 'n' will be omitted hereafter.

Convection fluxes

The convection terms in the continuity equation (1b) represent the mass fluxes through the CV faces. Here only the 'e' face will be considered (see Figure 1), the other faces being treated in an analogous way. By assuming that the CV vertices are connected by straight lines, the surface vector $\mathbf{S}_\mathrm{e}$ can be defined as

$$\mathbf{S}_\mathrm{e} = (y_\mathrm{n} - y_\mathrm{s})_\mathrm{e}\mathbf{i} - (x_\mathrm{n} - x_\mathrm{s})_\mathrm{e}\mathbf{j}, \tag{11}$$

which may also be interpreted as being an average surface vector for an (arbitrary) curved surface connecting the two CV vertices. The mass flux can then be evaluated, taking into account expression (8), as

$$\int_{S_\mathrm{e}} \rho(\mathbf{v} - \mathbf{v}_\mathrm{b})\cdot \mathrm{d}\mathbf{S} \approx \rho_\mathrm{e}(\mathbf{v}\cdot\mathbf{S} - \mathbf{v}_\mathrm{b}\cdot\mathbf{S})_\mathrm{e} = \rho_\mathrm{e}\left[\,[u(y_\mathrm{n} - y_\mathrm{s}) - v(x_\mathrm{n} - x_\mathrm{s})] - \frac{\delta V}{\delta t}\right]_\mathrm{e} = F_\mathrm{e}. \tag{12}$$

The velocity components at the CV faces, needed for the evaluation of the mass fluxes, are obtained from a special interpolation practice which assures a stable solution procedure with

collocated grids, as described in the text section. The volume change is calculated from the co-ordinates of the CV vertices at the two time levels, as described before.

The convection flux of variable ϕ through the CV face 'e' may now be evaluated as follows:

$$C_e = \int_{S_e} \rho\phi(\mathbf{v} - \mathbf{v}_b)\cdot d\mathbf{S} \approx \rho_e\phi_e(\mathbf{v}\cdot\mathbf{S} - \mathbf{v}_b\cdot\mathbf{S})_e \approx F_e\phi_e, \tag{13}$$

where ϕ_e stands for the cell face mean value of the variable ϕ. Here a second-order central differencing scheme (CDS), which implies linear interpolation, is used to express it via the neighbouring nodal values. The CDS is implemented using the 'deferred correction' approach, first suggested by Khosla and Rubin.[19] The convection flux is split into an 'implicit' part, expressed through first-order upwind differencing (UDS), and an explicit part, which equals the difference between the CDS and UDS approximations:

$$(F\phi)_e = (F\phi)_e^{UDS} + \gamma[(F\phi)_e^{CDS} - (\mathbf{F}\phi)_e^{UDS}]. \tag{14}$$

Multiplication of the explicit part by a factor γ ($0 \le \gamma \le 1$) allows the introduction of numerical diffusion ($\gamma = 0$ means pure UDS approximation), as may be necessary to damp wiggles resulting in some cases from the use of CDS on coarse grids. The deferred correction approach enhances the diagonal dominance of the coefficient matrix, which adds to the stability of the solution algorithm.

Diffusion fluxes

The diffusion flux of ϕ through the 'e' cell face can, after applying some vector algebra in order to express the gradient operator in terms of derivatives along the co-ordinate lines, be evaluated as follows:

$$D_e = -\int_{S_e} \Gamma\phi \operatorname{grad}\phi\cdot d\mathbf{S} \approx -\left[\frac{\Gamma_\phi}{V}\right]_e [(\phi_E - \phi_P)(\mathbf{S}_e\cdot\mathbf{S}_e) + \underline{(\phi_n - \phi_s)(\mathbf{S}_e\cdot\mathbf{S}_n)}]_e. \tag{15}$$

In the above expression the volume V_e equals the scalar product of the surface vector $\mathbf{S}_e$ and the distance vector $\overrightarrow{PE}$; $(\mathbf{S}_n)_e$ is the surface vector defining the segment of surface η = const bounded by nodes P and E (see Figure 1), directed as $\mathbf{S}_n$, i.e.

$$(\mathbf{S}_n)_e = -(y_E - y_P)\mathbf{i} + (x_E - x_P)\mathbf{j}. \tag{16}$$

The underlined part of the diffusion flux in equation (15) is usually called the 'cross-diffusion' contribution. It vanishes when the grid is orthogonal, and is small compared to the other part if the grid non-orthogonality is not severe; for this reason it is treated explicitly. This simplifies the coefficient matrix, since only the contributions of the four immediate neighbours of node P are then treated implicitly. In the case of the momentum component equations, the extra term which does not feature in the model equation (9) is also treated explicitly, as an extra source, as will be explained shortly. This renders the coefficients of the discretized equations equal for all the velocity components.

Sources

The source term is to be integrated over the cell volume, as indicated in equation (9). By assuming—implying indirectly the mean value theorem—that the specific source at the CV centre represents the mean value over the whole control volume, one can write

$$S_\phi = \int_V s_\phi \, dV \approx (s_\phi)_P V. \tag{17}$$

Apart from the 'real' source s_ϕ, explicitly treated parts of the convection and diffusion fluxes may also be added to s_ϕ. The momentum component equations are a special case since they contain an extra term not featured in equation (9). This term is also treated explicitly ; its discretization is analogous to that of the 'ordinary' diffusion flux, i.e.

$$S_{u_i}^{\tau} = \int_S [-(p + \tfrac{2}{3}\mu \operatorname{div} \mathbf{V})\mathbf{i}_i + \mu(\operatorname{grad} \mathbf{v})^{\mathrm{T}} \cdot \mathbf{i}_i] \cdot \mathrm{d}\mathbf{S} \approx \sum_j [-(p + \tfrac{2}{3}\mu \operatorname{div} \mathbf{v})\mathbf{i}_i + \mu(\operatorname{grad} \mathbf{v})^{\mathrm{T}} \cdot \mathbf{i}_i] \cdot \mathbf{S}_j. \tag{18}$$

Boundary conditions

The expressions for the evaluation of the convective and diffusive fluxes described above are valid for all interior CV faces. On the faces coinciding with the boundary of the solution domain, appropriate boundary conditions have to be applied in order to make the resulting system of algebraic equations solvable. Basically two kinds of boundary conditions may apply: (i) the boundary fluxes are known, in which case they are added to the source terms of adjacent control volumes and the above flux evaluation formulae are suppressed for the boundary cell faces, or (ii) the boundary values of the dependent variable ϕ are known, in which case the above formulae are applied for the evaluation of the fluxes. In the case where the boundary fluxes are prescribed (e.g. zero fluxes through the symmetry plane), the values of the variables at the boundary nodes have to be evaluated by means of a suitable extrapolation procedure from the interior nodal values, since they are needed for the evaluation of the cross-diffusion fluxes through the faces adjacent to the boundary. Details on the treatment of various kinds of boundaries may be found in Perić.[17]

System of algebraic equations

Summing the fluxes through all faces of one CV results in an algebraic equation which links the value of the dependent variable at the CV centre with the neighbouring values:

$$A_{\mathrm{P}}\phi_{\mathrm{P}} = \sum_{\mathrm{nb}} A_{\mathrm{nb}}\phi_{\mathrm{nb}} + Q_\phi, \quad \mathrm{nb} = \mathrm{E, W, N, S.} \tag{19}$$

The coefficients A_{nb} contain contributions from the convection and diffusion fluxes as defined by equation (13) and (15). The central coefficient A_{P} can, by employing the discretized continuity equation (23), be expressed in the following way:

$$A_{\mathrm{P}} = \sum_{\mathrm{nb}} A_{\mathrm{nb}} + \frac{(\rho V)^{\circ}}{\delta t} \tag{20}$$

For the solution domain as a whole there results a system of N equations with N unknowns, where N is the number of control volumes. The coefficient matrix of such a system has non-zero coefficients only on five diagonals. Several efficient iterative solvers can be employed to solve the system of equations; in this study the strongly implicit procedure (SIP) of Stone,[20] based on an incomplete LU factorization of the coefficient matrix, is used. If the source term is a function of ϕ, a suitable linearization may provide another *positive* contribution to the central coefficient. This enhances the diagonal dominance of the coefficient matrix, which makes the iterative solution procedure more stable. Another way of enhancing the stability of the solution method, especially when the equations are non-linear and coupled, is underrelaxation. More details on the above techniques can be found in many publications, e.g. in Patankar.[21]

PRESSURE–VELOCITY COUPLING AND SOLUTION ALGORITHM

Pressure correction equation

The coupling of pressure and velocities is achieved via the well known SIMPLE algorithm.[22] The continuity equation is thus transformed into a pressure correction equation which has the same general form as the other discretized equations (equation (19)). Details concerning the derivation of this equation for a collocated arrangement of variables can be found in Perić;[17] here only a brief summary will be given.

For the calculation of the mass fluxes through the CV faces and for checking mass conservation, the values of the velocity components at the CV face centres are needed. In order to avoid oscillations which may result if a simple linear interpolation is used for this purpose, a special interpolation practice is employed, as suggested by Prakash,[23] Hsu[24] and Rhie.[25] The basis for this interpolation are the discretized momentum equations at the CV centres on either side of the face in question, which may be rewritten as follows:

$$u_P^* = \frac{\Sigma A_{nb} u_{nb}^* + Q_u^*}{A_P} + d_P(P_e^* - P_w^*). \tag{21}$$

Here the pressure difference in the w–e direction has been taken out of the Q-term and shown explicitly. The superscript asterisk denotes values employed in and resulting from the momentum equations. To evaluate u_e^*, terms on the right-hand side of equation (20) are selectively interpolated for or evaluated at the 'e' location; thus

$$u_e^* = \left[\frac{\overline{\Sigma A_{nb} u_{nb}^* + Q_u^*}}{A_P}\right]_e + \bar{d}_e(P_E^* - P_P^*), \tag{22}$$

where the overbar denotes linear interpolation. The cell face velocities are thus made dependent on the pressures at the two neighbouring nodes, as is the case in the *true* staggered arrangement.

From now on the SIMPLE strategy can be used in its standard form, developed for the staggered arrangement of velocities and pressure. The mass imbalance, which results when the cell face velocity components u_i^*, calculated from expressions like (22), are introduced in the continuity equation (see equation (1b)),

$$\frac{(\rho V)^n - (\rho V)^o}{\delta t} + F_e^* + F_w^* + F_n^* + F_s^* = S_m, \tag{23}$$

is to be annihilated by the mass flux corrections F'. These are based on the velocity corrections u', which are further related to the pressure corrections P' by, e.g. at the 'e' face,

$$u_e' = \bar{d}_e(P_E' - P_P'). \tag{24}$$

The continuity equation then reads

$$F_e' + F_w' + F_n' + F_s' + S_m = 0, \tag{25}$$

which eventually leads to an equation for the pressure correction which has the same form as equation (19). Note that, for example, F_w for the cell centred around node P is equal to $-F_e$ of the cell centred around node W.

The extension of the pressure correction approach for the collocated arrangement of variables to the PISO algorithm of Issa,[26] as well as to other related coupling algorithms such as SIMPLER[21] or SIMPLEC,[27] is also straightforward, as described by Perić.[17] It should also be

noted that the underrelaxation factors for the velocity components, inherent in equation (21), affect the values of the cell face velocities when the pressure variation is non-linear. A study of this effect and a possibility for its suppression are presented by Majumdar.[28]

Solution algorithm

The solution algorithm for the calculation of unsteady flows in irregular domains with moving boundaries can be summarized as follows.

1. Provide the initial grid and values of the dependent variables (solution for time t_0);
2. Determine the location of the boundary grid points after the time has advanced by δt and move the old grid to fit the new boundaries. It is assumed here that the law which governs the motion of the solution domain boundary is known, either as a function of time alone (externally induced boundary motion, e.g. in a piston/cylinder assembly) or as a function of the previous flow development (internally induced boundary motion, e.g. in free surface flows). The number of control volumes is thereby kept constant.
3. Assemble and solve the equations for the velocity components, employing the currently available pressure *and mass fluxes*. One pass in the SIP solver is often sufficient.
4. Calculate the new mass fluxes using the new velocity components and determine the mass imbalance in each CV.
5. Assemble and solve the pressure correction equation. Apply SIP until the sum of the absolute residuals is reduced by a factor of four to five.
6. Correct the mass fluxes, nodal velocity components and pressure by the calculated pressure correction.
7. Assemble and solve any other scalar equation which may be coupled with the momentum equations (e.g. temperature, turbulent kinetice energy and its dissipation rate, etc.) and update the fluid properties (density, viscosity) if necessary.
8. Return to step 3 and repeat until the sum of the absolute residuals in the momentum and continuity equations has fallen by two to three orders of magnitude.
9. Advance the time by another increment δt and returen to step 2; repeat until the prescribed number of time steps is completed.

The number of iterations per time step (steps 3–7) depends on the size of the time increment δt; for smaller δt fewer iterations are needed to reach the solution at the new time level. The number of iterations and the computing time can be reduced considerably by employing multigrid coupling, as done for orthogonal grids by Barcus *et al.*,[29] Becker *et al.*[30] and Durst *et al.*[31]

APPLICATION OF THE METHOD

The present method is an extension of the method developed for steady flows by Perić.[17] He has demonstrated the suitability of the method for the prediction of flows in complex geometries by applying it to a number of test cases in both two and three dimensions. The relative merits of staggered and collocated variable arrangements are studied on several flows in rectangular geometries by Perić *et al.*[32] The role of the space conservation law in numerical calculations with moving grids has previously been studied by Demirdžić and Perić.[13]. For the sake of demonstrating the ability of the present method to predict the flow in complex geometries with moving boundaries, we have performed calculations for the flow in a channel with a moving indentation, which has been studied experimentally by Pedley and Stephanoff[33] and numerically by Ralph and Pedley.[11]

Description of problem

The geometry of the flow domain is shown in Figure 3. The shape of the indentation is taken from Pedley and Stephanoff,[33] who specified analytic functions which approximately fit the real shape used in the experiment. The height of the bottom (indented) wall is given by

$$y(x) = \begin{cases} h & \text{for } 0 < x < x_1, \\ 0{\cdot}5h\{1 - \tanh[a(x - x_2)]\} & \text{for } x_1 < x < x_3, \\ 0 & \text{for } x > x_3, \end{cases} \tag{26}$$

where $a = 4{\cdot}14$, $x_1 = 4b$, $x_3 = 6{\cdot}5b$, $x_2 = 0{\cdot}5(x_1 + x_3)$ and

$$h = 0{\cdot}5h_{\max}[1 - \cos(2\pi t^*)], \qquad t^* = (t - t_0)/T. \tag{27}$$

Here b is the channel height, T is the oscillation period and $h_{\max} = 0{\cdot}38b$ specifies the maximum blockage of the channel cross-section at $t^* = 0{\cdot}5$. The geometry is symmetric around $x = 0$, i.e. $y(-x) = y(x)$. The Strouhal number, based on the channel height b, bulk velocity U and oscillation period T,

$$St = b/UT, \tag{28}$$

was 0·037. The Reynolds number, based on the above reference quantities, was 507.

At $t = t_0$ (initial state) the flow is assumed to be fully developed. The velocity profile at the inlet cross-section is taken to remain constant throughout the cycle, which is approximately in accordance with experiment. At the other channel end, zero gradient in the x-direction for both velocity components is taken as the boundary condition. The effect of this—definitely not perfect—boundary condition on the solution was not studied; it can be anticipated that in the second half of the period the region near the exit may be affected. This could have been checked by placing the outlet boundary at various locations downstream of the indentation, as done by Ralph and Pedley.[11] However, since the experiments offer no quantitative data for detailed validation of the numerical solution, no effort in this direction has been made here. All time step and grid size dependence tests were carried out with the same boundary conditions.

Grid dependence tests

Calculations were performed on two numerical grids covering the region shown in Figure 3: one coarse with a 91 × 20 CV, and one refined with a 221 × 40 CV. One section of the fine grid at

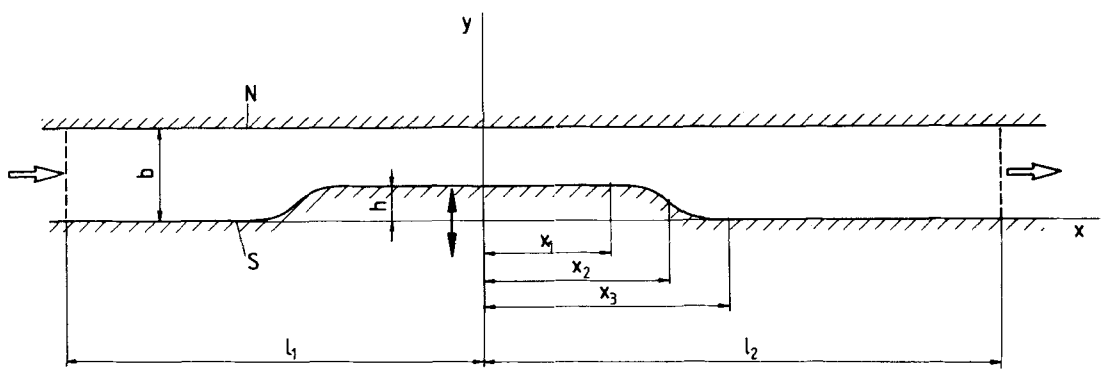

Figure 3. Geometry of the test case (not to scale): $b = 1$ cm, $l_1 = 9{\cdot}85$ cm, $l_2 = 18{\cdot}0$ cm

$t^* = 0$ and $t^* = 0{\cdot}5$ is shown in Figure 4 (to scale). In the region around the indentation ends the grid is non-orthogonal and non-uniform; in the rest of the solution domain it is orthogonal and uniform but not square. Pure central differences are used in both cases for the discretization of the convection fluxes ($\gamma = 1$ in equation (14)). Two time increments were used for the coarse grid calculations: $\delta t = T/50$ and $\delta t = T/200$. Fine grid calculations were carried out only with the smaller time increment. Typically 40 iterations per time step were performed and the computing time per iteration was about 1·6 s on a Cyber 205 computer.

Figure 5 shows a comparison of the wall shear stresses calculated on the coarse grid with two different time steps at $t^* = 0{\cdot}5$. Differences between the two solutions exist only in the region downstream of the indentation. The magnitudes of the peaks are higher for smaller δt, but no significant changes in the position of separation and reattachment can be observed. This indicates

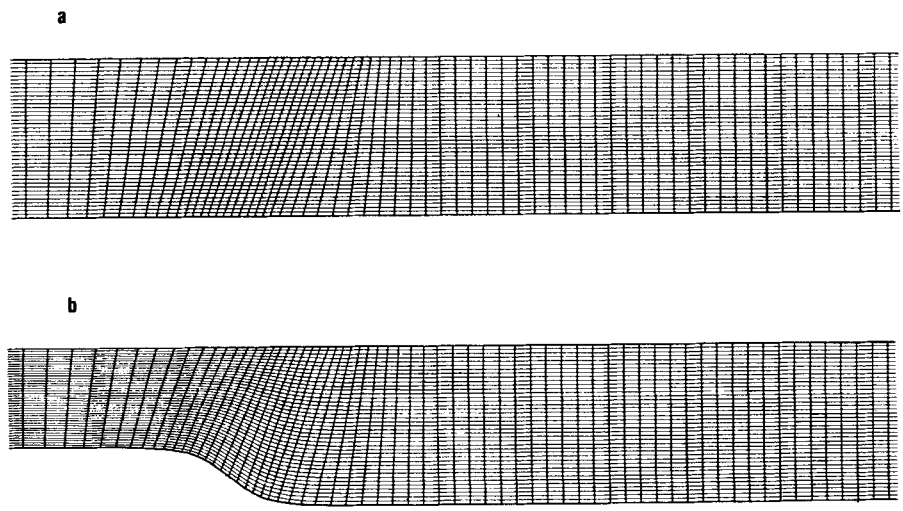

Figure 4. Section of the fine grid (221 × 40 CV) at (a) $t^* = 0$ and (b) $t^* = 0{\cdot}5$

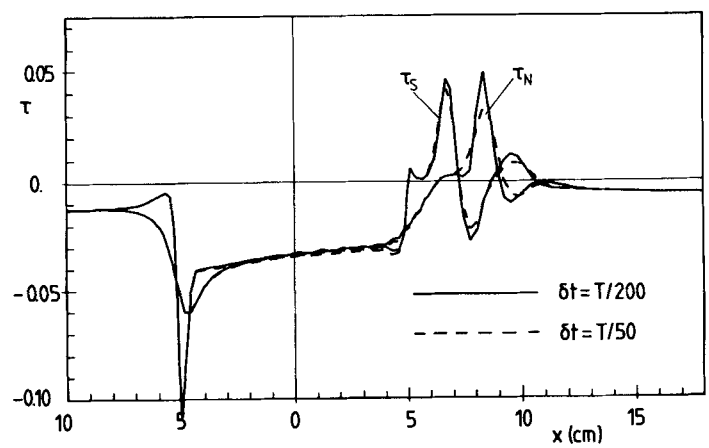

Figure 5. Comparison of predicted wall shear stresses at $t^* = 0{\cdot}5$ using the coarse (91 × 20 CV) grid and various time steps

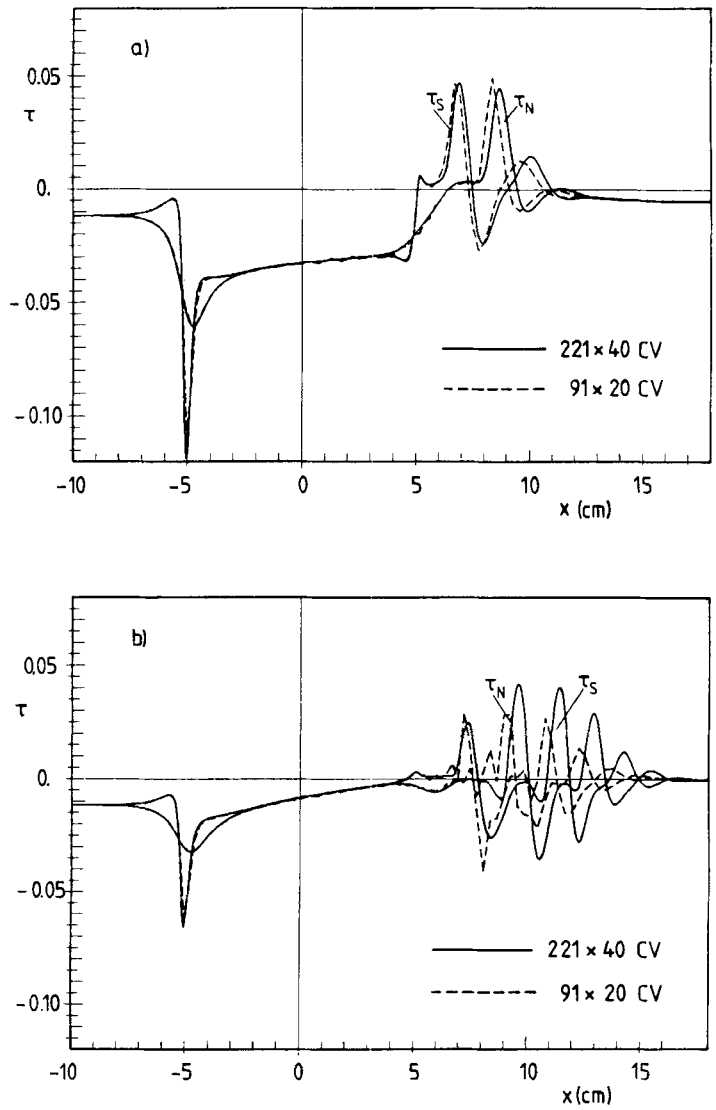

Figure 6. Comparison of predicted wall shear stresses on two grids at (a) $t^* = 0{\cdot}5$ and (b) $t^* = 0{\cdot}7$ using time step $\delta t = T/200$

that the temporal discretization errors are smaller than the spatial ones. This is demonstrated in Figures 6(a) and 6(b), where comparisons between fine and coarse grid results at $t^* = 0{\cdot}5$ and $t^* = 0{\cdot}7$ respectively (both obtained with $\delta t = T/200$) are presented. Significant differences exist, especially for $t^* > 0{\cdot}5$. These comparisons show that the finer grid is still not fine enough to provide grid-independent results. The smaller of the two time steps can be considered adequate for the spatial resolution of the grid employed. Although for numerically accurate results further grid refinement is necessary, for the sake of qualitative comparison with the flow visualization results of Pedley and Stephanoff[33] the numerical accuracy achieved on the 221 × 40 CV and $\delta t = T/200$ suffices.

Results of calculations

Figures 7(a)–7(i) show predicted velocity vectors, isobars and streamlines at $t^* = 0{\cdot}2$, 0·3, 0·4, 0·5, 0·6, 0·7, 0·8, 0·9 and 1·0 respectively. Only the section behind the indentation is shown since the flow upstream of it is not much affected by its movement. In this region an undisturbed fully developed flow regime prevails. Owing to the displacement of fluid by the moving indentation, the flow rate behind it is higher than the (constant) inlet rate for $t^* < 0{\cdot}5$. The maximum velocity occurs at $t^* = 0{\cdot}4$, exceeding the maximum velocity of the fully developed flow by 76% (2·645 versus 1·5). For $t^* > 0{\cdot}5$ the oncoming fluid fills the gap left by the retracting indentation, so that the outgoing flow rate reduces below the incoming one. The maximum velocity becomes closer to that of the fully developed flow as the end of the period is approached. The first separation occurs behind the indentation between $t^* = 0{\cdot}2$ and 0·25. Between $t^* = 0{\cdot}35$ and 0·4 another vortex appears at the opposite wall, shifted about one channel height downstream. At about $t^* = 0{\cdot}45$ the third vortex appears behind the first one. The vortices continue building up alternately at the upper and lower wall until there are four of them at each wall. They move with the flow, the downstream ones somewhat faster; at the same time they grow stronger, but after $t^* \approx 0{\cdot}7$ they begin to weaken, dying out completely after $t^* = 0{\cdot}9$, so that at $t^* = 1{\cdot}0$ only slightly wavy streamlines remain. The pressure also recovers very quickly from a very complex structure at $t^* = 0{\cdot}8$ to a nearly uniform distribution at the cycle end.

Figures 8(a) and 8(b) show the variation of the wall shear stress on the lower (indented) and upper wall respectively during the cycle. They indicate the strength of the eddies, the positions of separation and reattachment (change of sign in wall shear stress) and thus the movement of eddies along the wall. The first four eddies, marked A, B, C and D in Figure 7(e), are the strongest; eddies E and F are relatively weak. The last two eddies might have been weakened by the simple outflow boundary condition employed in the calculations. However, experiments and recent calculations of Ralph and Pedley[11] also indicate weaker eddies in this region. Eddy A is strongest at $t^* = 0{\cdot}5$ (maximum shear stress occurs then); peaks in other eddies occur $0{\cdot}05T$ later, in the order of their appearance. The shear stress variation along the indentation and the opposite wall also indicates an acceleration of the flow in this region when the indentation is moving inwards ($t^* < 0{\cdot}5$; $d\tau/dx < 0$) and a deceleration when it is retracting ($t^* > 0{\cdot}5$; $d\tau/dx > 0$). The steadiness of the flow in front of the indentation is also evident from Figure 8.

Discussion

The flow structure observed in our prediction on a 221 × 40 CV grid is qualitatively in good agreement with both the experimental study of Pedley and Stephanoff[33] and the recent numerical results of Ralph and Pedley.[1] The solution procedure used by Ralph and Pedley[11] was a finite difference method in a streamfunction–vorticity formulation, specially modified for this case. (The co-ordinate transformation which they used in this adaptation can be applied only for mildly curved and moderately steep indentations; it will become singular in the case of a step-like indentation.) They used uniform square grids, except in the region of indentation where the grid was square only in the transformed space. Their finest grid had about seven times as many nodes in the x-direction as the one used in this study. Since they used an explicit scheme, for stability reasons they had to use very small time increments, $\delta t = T/6000$. It should be noted that their finite difference procedure takes no account of the space conservation law. However, owing to the very small time step size employed, the space conservation errors are most probably negligible according to the analysis of Demirdžić and Perić.[13]

Although the grid employed here was significantly coarser and the time step 30 times longer than in the above referenced study, the qualitative agreement of the two predictions is good. All

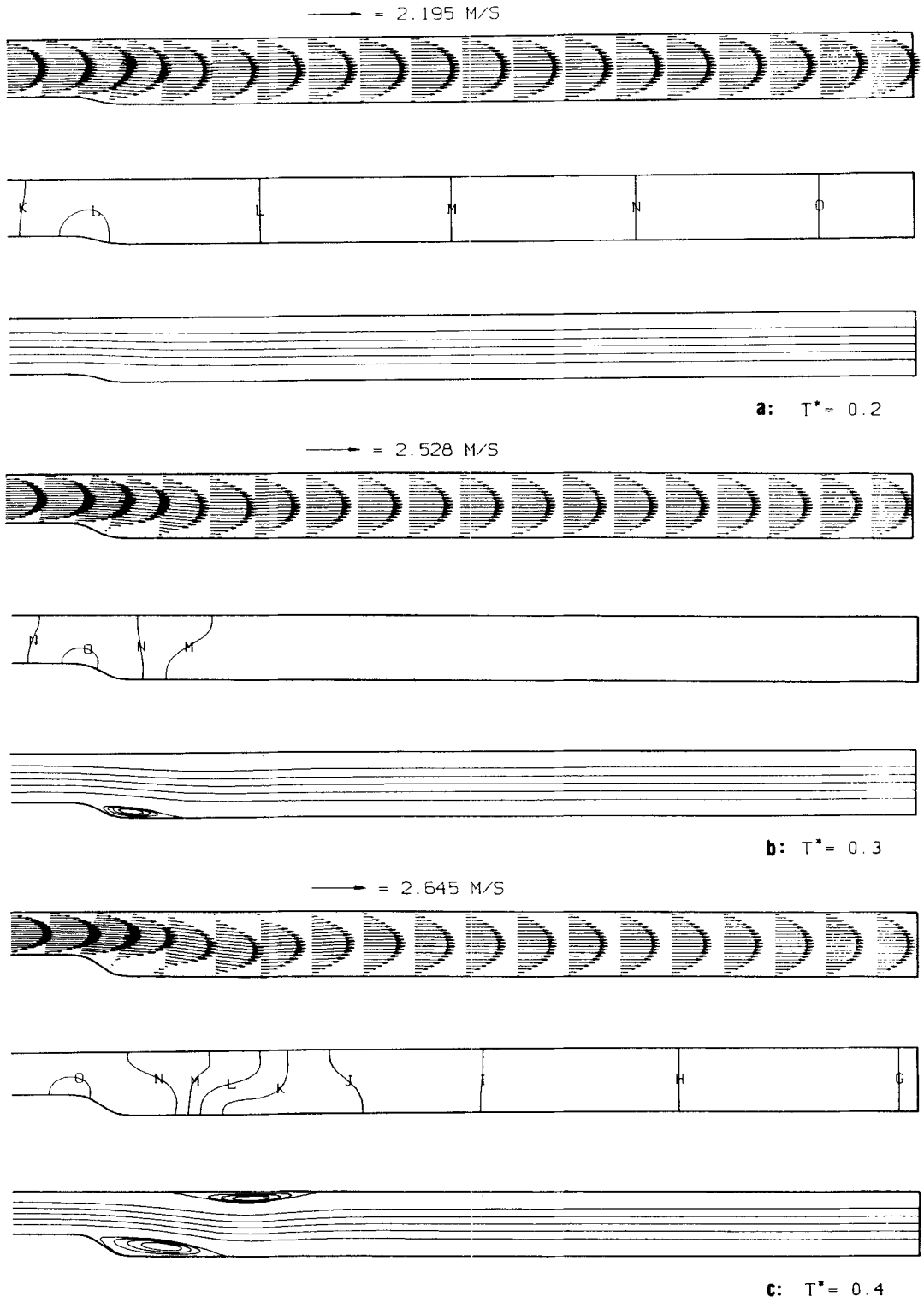

Figure 7. (a–c)

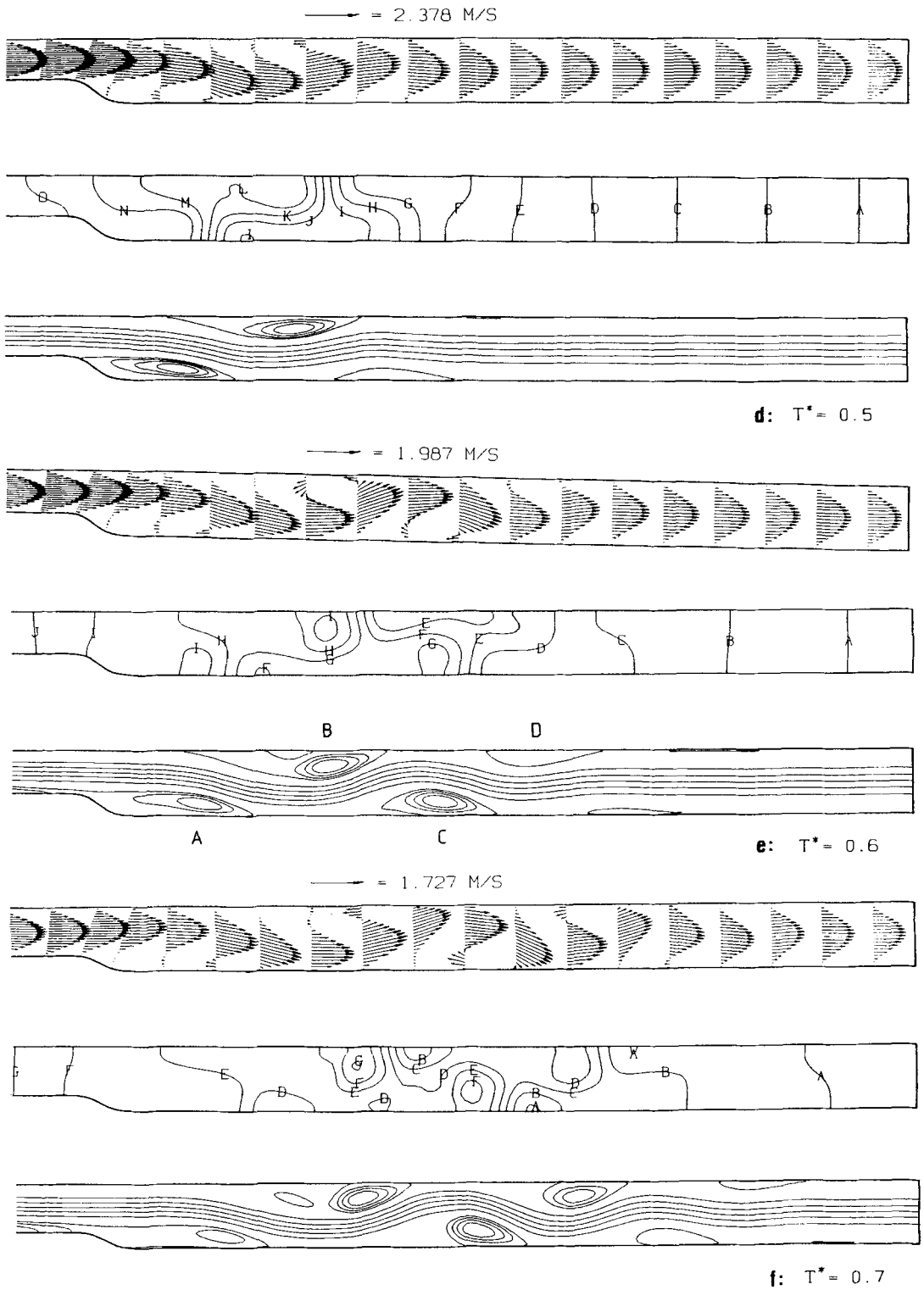

Figure 7. (d–f)

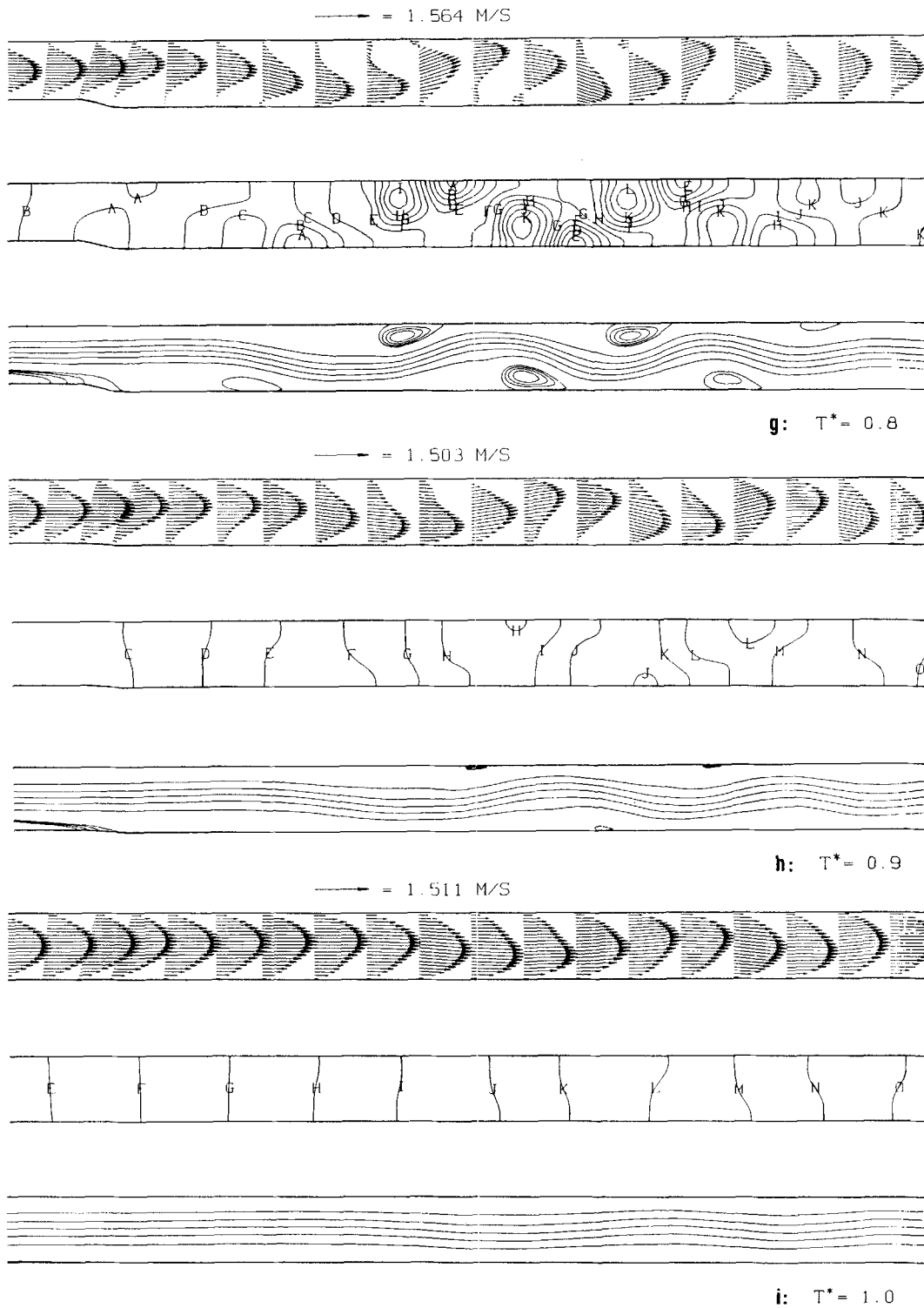

Figure 7. Predicted velocity vectors, isobars and streamlines downstream of indentation at various times t^*: (a) 0·2; (b) 0·3; (c) 0·4; (d) 0·5; (e) 0·6; (f) 0·7; (g) 0·8; (h) 0·9; (i) 1·0

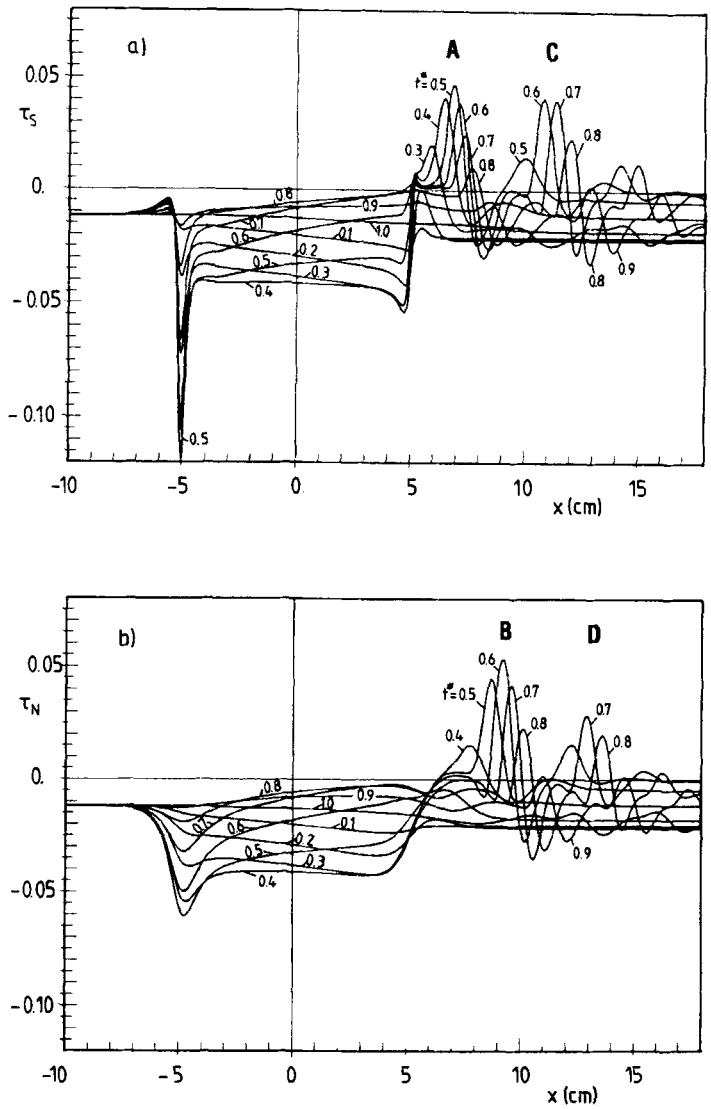

Figure 8. Predicted wall shear stress variation during one cycle: (a) indented wall (τ_S); (b) opposite wall (τ_N)

the important flow phenomena reported in the above cited studies have been observed in the present prediction too. The most remarkable effect is the break-up of eddy B; see Figures 7(d)–7(f). This phenomenon is discussed in detail by Ralph and Pedley.[11] Figure 9 shows the only possible quantitative comparison of experiment and prediction. The positions of wave crests and troughs corresponding to eddies B, C and D have been evaluated from the flow visualization photographs and presented by Pedley and Stephanoff.[33] The same information evaluated from the predicted streamline plots is compared with the experimentally observed values in Figure 9. The positions of the horizontal tangent to the upper and lower of the five core streamlines (see Figures 7(d)–7(i)) are read visually from the streamline plots, the process being assisted by the resolution of the laser printer (300 dots per inch), which shows at those places a small portion of streamline as a straight horizontal line. The values obtained for the two streamlines determine the borders of the shaded

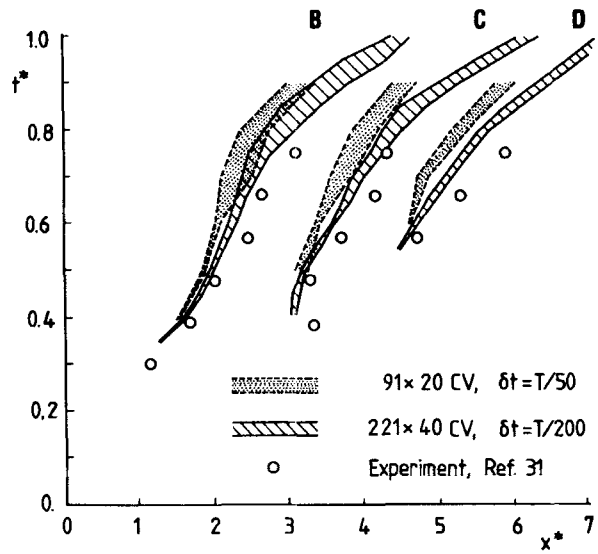

Figure 9. Comparison of predicted and experimentally observed positions of wave crests and troughs correponding to eddies B, C and D as functions of time

area in Figure 9. According to Pedley and Stephanoff,[33] the abscissa is defined as

$$x^* = (x - x_1)(10St)^{1/3}/b. \tag{29}$$

One can see from this figure that the wave length is correctly predicted, the prediction lines being always to the left of the experimental data. The effect of grid refinement is also obvious: find grid results are always closer to the experimental data. However, in order to obtain grid-independent results, further refinement, both spatial and temporal, is necessary. This has not been pursued here owing to the lack of computational resources and more detailed, quantitative experimental data.

CONCLUSIONS

In this paper a finite volume method for the prediction of fluid flow in arbitrarily shaped domains with moving boundaries is presented. The method is both Lagrangian and Eulerians since the numerical mesh may move with the fluid (Lagrangian approach), be held fixed (Eulerian approach) or be moved in any other prescribed way. Fully implicit temporal and central differencing spatial discretization are employed. The method is fully conservative, since the strong conservation form of the governing equations (with Cartesian velocity components) is used and the space conservation law is acccounted for in the discretization process.

The advantages of the present method over explicit finite difference methods, as used e.g. by Ralph and Pedley,[11] are the following:

(1) use of non-orthogonal boundary-fitted grids, which makes the treatment of complex boundaries (e.g. with discontinuities) relatively easy
(2) use of a collocated variable arrangement, which makes the extension to three dimensions and the employment of multigrid methods less complicated than when the staggered arrangement is used

(3) fully conservative discretization
(4) no restriction to the time step size as in explicit methods, which allows efficient calculation of flows requiring finer spatial than temporal discretization (e.g. flows approaching steady state).

Comparisons of predictions for a flow in a channel with moving indentation with experimental observations and another numerical study with much finer spatial and temporal resolution are favourable.

Further development of the method includes implementation of the multigrid coupling procedure in order to reduce the computing effort per time step, as reported by Durst *et al.*[31] in applications to orthogonal grids.

ACKNOWLEDGEMENTS

The authors thank A. D. Gosman and R. I. Issa for their contribution to the development of the present method. This work was sponsored by the Deutsche Forschungsgemeinschaft and partially by the Internationales Büro, KFA Jülich, through a grant to I. Demirdžić. We greatly appreciate this support.

REFERENCES

1. J. A. Viecelly, 'A computing method for incompressible flows bounded by moving walls', *J. Comput. Phys.*, **8**, 119–143 (1979).
2. F. H. Harlow and J. E. Welch, 'Numerical calculation of time-dependent viscous incompressible flow of fluid with free surface', *Phys. Fluids*, **8**(12), 2182–2189 (1965).
3. S. K. Godunov and G. P. Prokopov, 'The use of moving meshes in gas-dynamical computations', *Zh. Vychisl. Mater. Mater. Fiz.*, **12**(2), 429–440 (1972).
4. C. W. Hirt, A. A. Amsden and J. L. Cook, 'An arbitrary Lagrangian–Eulerian computing method for all flow speads', *J. Comput. Phys.*, **14**, 227–253 (1974).
5. A. D. Gosman and A. P. Watkins, 'A computer prediction method for turbulent flow and heat transfer in piston/cylinder assemblies', in *Proc. 1st Symp. on Turbulent Shear Flows*, The Pennsylvania State University, Pennsylvania, USA, 18–20 April, 1977, p. 523.
6. A. D. Gosman and R. J. Johns, 'Development of a predictive tool for in-cylinder gas motion in engines', *SAE Paper 780315*, 1978.
7. A. D. Gosman, 'Prediction of in-cylinder processes in reciprocating internal combustion engines', in R. Glowinski and J.-L. Lions (eds), *Computing Methods in Applied Sciences and Engineering, VI*, Elsevier (North-Holland), Amsterdam, 1984, pp. 609–629.
8. P. D. Thomas and C. K. Lombard, 'Geometric conservation law and its application to flow computations on moving grids', *AIAA J.*, **17**, 1030–1037 (1979).
9. S. C. Ling and H. B. Atabek, 'A nonlinear analysis of pulsatile flow in arteries', *J. Fluid Mech.*, **55**, 493–511 (1972).
10. E. Krause, 'The computation of three-dimensional viscous flows', in W. Kollmann (ed.), *Computational Fluid Dynamics*, Hemisphere, New York, 1980, pp. 67–92.
11. M. E. Ralph and T. J. Pedley, 'Flow in a channel with a moving indentation', *J. Fluid Mech.*, **190**, 87–112 (1988).
12. F. Durst, J. C. F. Pereira and G. Scheuerer, 'Calculations and experimental investigations of the laminar unsteady flow in a pipe expansion', in E. H. Hirschel (ed.), *Finite Approximations in Fluid Mechanics*, Vieweg, Braunschweig, 1985, pp. 43–55.
13. I. Demirdžić and M. Perić, 'Space conservation law in finite volume calculations of fluid flow', *Int. j. numer. methods fluids*, **8**, 1037–1050 (1988).
14. J. F. Thompson (ed.), *Numerical Grid Generation*, North-Holland, New York, 1982.
15. G. S. Deiwert and H. Rothmund, 'Three dimensional flow over a conical afterbody containing a centered propulsive jet: a numerical simulation', *AIAA Paper 83–1709*, 1983.
16. C. M. Hung and P. G. Buning, 'Simulation of blunt-fin induced shock wave and turbulent boundary layer interaction', *AIAA Paper 84–0457*, 1984.
17. M. Perić, 'A finite volume method for the prediction of three-dimensional fluid flow in complex ducts', *Ph.D. Thesis*, University of London, 1985.
18. J. C. Slattery, *Momentum, Energy and Mass Transfer in Continua*, McGraw-Hill, New York, 1972.
19. P. K. Khosla and S. G. Rubin, 'A diagonally dominant second-order accurate implicit scheme', *Comput. Fluids*, **2**, 207–209 (1974).

20. H. L. Stone, 'Iterative solution of implicit approximations of multidimensional partial differential equations', *SIAM J. Numer. Anal.*, **5**, 530–558 (1968).
21. S. V. Patankar, *Numerical Heat Transfer and Fluid Flow*, McGraw-Hill, New York, 1980.
22. S. V. Patankar and D. B. Spalding, 'A calculation procedure for heat, mass and momentum transfer in three-dimensional parabolic flows', *Int. J. Heat Mass Transfer*, **15**, 1787–1806 (1972).
23. C. Prakash, 'A finite element method for predicting flow through ducts with arbitrary cross sections', *Ph.D. Thesis*, University of Minnesota, 1981.
24. C. Hsu, 'A curvilinear-coordinate method for momentum, heat and mass transfer in domains of irregular geometry', *Ph.D. Thesis*, University of Minnesota, 1981.
25. C. M. Rhie, 'A numerical study of the flow past an isolated airfoil with separation', *Ph.D. Thesis*, University of Illinois, Urbana-Champaign, 1981.
26. R. I. Issa, 'Solution of the implicitly discretized fluid flow equations by operator-splitting', *J. Comput. Phys.*, **62**, 40–65 (1986).
27. J. P. Van Doormal and G. D. Raithby, 'Enhancements of the SIMPLE method for predicting incompressible fluid flows', *Numer. Heat Transfer*, **7**, 147–163 (1984).
28. S. Majumdar, 'Role of underrelaxation in momentum interpolation for calculation of flow with nonstaggered grids', *Numer. Heat Transfer*, **13**, 125–132 (1988).
29. M. Barcus, M. Perić and G. Scheuerer, 'A control volume based full multigrid procedure for the prediction of two-dimensional, laminar incompressible flows', in M. Deville (ed.), *Notes on Numerical Fluid Mechanics, Vol. 20*, Vieweg, Braunschweig, 1988, pp. 9–16.
30. C. Becker, J. H. Ferziger, M. Perić and G. Scheuerer, 'Finite volume multigrid solutions of the two-dimensional incompressible Navier–Stokes equations', in W. Hackbusch (ed.), *Notes on Numerical Fluid Mechanics, Vol. 23*, Vieweg, Braunschweig, 1988, pp. 37–47.
31. F. Durst, M. Perić, G. Scheuerer and H. Ströll, 'Numerical study of laminar, unsteady piston-cylinder flows', in E. H. Hirschel (ed.), *Notes on Numerical Fluid Mechanics, Vol. 25*, Vieweg, Braunschweig, 1989, pp. 80–92.
32. M. Perić, R. Kessler and G. Scheuerer, 'Comparison of finite-volume numerical methods with staggered and colocated grids', *Comput. Fluids*, **16**, 389–403 (1988).
33. T. J. Pedley and K. D. Stephanoff, 'Flow along a channel with a time-dependent indentation in one wall: the generation of vorticity waves', *J. Fluid Mech.*, **160**, 337–367 (1985).